Journal of South American Earth Sciences 103 (2020) 102799

Contents lists available at ScienceDirect

Journal of South American Earth Sciences

journal homepage: www.elsevier.com/locate/jsames

Seismicity along the Magallanes-Fagnano fault system

Jean-Baptiste Ammirati [a,*], M. Constanza Flores [b], Sergio Ruiz [c]

[a] Departamento de Geología, Facultad de Ciencias Físicas y Matemáticas, Universidad de Chile, Chile
[b] Centro Sismológico Nacional, Chile
[c] Departamento de Geofísica, Facultad de Ciencias Físicas y Matemáticas, Universidad de Chile, Chile

ARTICLE INFO

Keywords:
Tectonics
South America
Patagonia
Crustal earthquake
Surface wave
Body wave
Isostatic rebound

ABSTRACT

The Magallanes-Fagnano fault (at ~51-56°S) is a continental NW-SE transform fault zone that marks the boundary between the South American Plate (north) and the Scotia Plate (South). In 1949, two crustal seismic events of estimated magnitude M > 7 were located in this area using teleseismic records. Although, this region is scarcely populated, such shallow seismicity could represent a considerable threat to the remote urban centers in this sector. The characterization of the local seismicity always lacked good quality records and permanent instrumentation. In the recent past years, permanent seismic stations (CSN and INPRES-CTBTO) were deployed in the Tierra del Fuego Island and Southern Patagonia, providing with continuous time, broadband records of waveform data. In order to obtain better insights about the local seismicity associated with the Magallanes-Fagnano fault, we jointly inverted teleseismic receiver functions with Rayleigh-wave dispersion data to build a calibrated velocity model for the study region. In parallel, we analyzed the continuous waveforms to automatically detect local earthquakes and locate them using our regional velocity model. Our results show: 1) Shallow seismic events distributed along the Magallanes-Fagnano fault. 2) Diffuse seismicity characterizing the South American crust, north of 53°S. Our observations suggest two mechanisms of crustal deformation. In the Tierra del Fuego Island the seismicity is mostly associated with the Magallanes-Fagnano fault system. In the Southern Patagonia, along the Patagonian Andes the seismicity would be mostly due to isostatic rebound following the retreat of the Patagonian Ice sheet.

1. Introduction

The Southern Patagonia and the Tierra del Fuego Island (51-56°S) compose the south end of South America. This region is split by a ~600 km long, NW-SE lineament known as the Magallanes-Fagnano Fault System (MFFS). This large structure exhibits geomorphological and topographic features that generally characterize large scale transform system (Fuenzalida, 1976; Lodolo et al., 2003). These observations first suggested that the MFFS was the surface manifestation of the South America-Scotia plate boundary (Fig. 1). On the field, structural indicators evidenced left-lateral motion along the structure (Caminos et al., 1981; Winslow, 1982; Cunningham, 1993; Betka et al., 2016; Roy et al., 2019). Strike-slip focal mechanisms for earthquakes located on the northern Scotia ridge, south of Tierra del Fuego (TdF) confirmed this left lateral character along the MFFS (Pelayo and Wiens, 1989). More recently, geodetic observations put more constraints on the relative plate motion at the South America-Scotia plate boundary and have been able to quantify a relative velocity between the two plates of 6–7 mm/yr in the TdF Island where the MFFS shows an E-W orientation. (Smalley et al., 2003; Mendoza et al., 2011, 2015), although new evidence suggests a much higher rate (Sandoval and De Pascale., 2020). These observations thus demonstrate that the region is tectonically active although the lack of real-time seismological instrumentation at local scale did not allow to characterize the associated seismicity with much precision.

On February 1st' 1879, the population of Punta Arenas and Ushuaia, the two most important settlements located in this otherwise remote and scarcely populated region, reported a strong intensity earthquake (VII and VIII on the modified Mercalli scale, for the Punta Arenas and Ushuaia areas, respectively) (Cisternas and Vera, 2008). On December 17th' 1949, two earthquakes (at 6:53 GMT and 15:07 GMT, respectively) as well as several aftershocks stroke the same area. The magnitude, inferred from distant observations of the surface waves amplitudes associated with those two events, was respectively $M_S = 7.7$ and $M_S = 7.4$ (Geller and Kanamori, 1977; ISC, 2020). Because there are no seismological local records, the hypocentral locations of these events is only

* Corresponding author.
E-mail address: jbaptiste@ing.uchile.cl (J.-B. Ammirati).

https://doi.org/10.1016/j.jsames.2020.102799
Received 29 June 2020; Received in revised form 29 July 2020; Accepted 29 July 2020
Available online 2 August 2020

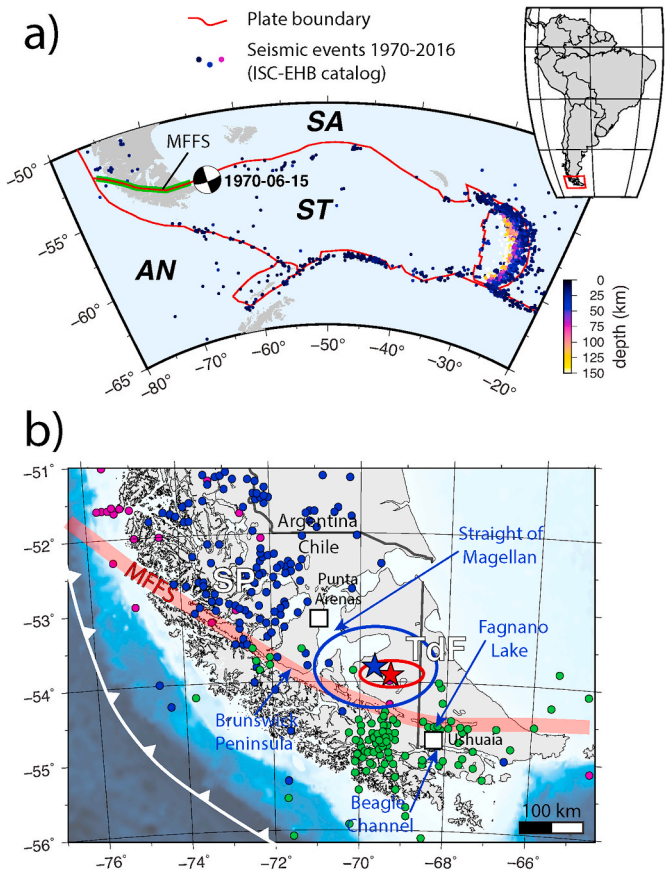

Fig. 1. a) General map showing the tectonic configuration of the southern tip of South America and Antarctica. Red lines show tectonic plates boundaries. The green line shows the Magallanes Fagnano Fault System (MFFS). Dots represent seismic events in the ISC-EHB catalog, for the 1970–2016 period (ISC, 2020). The focal mechanism is from Pelayo and Wiens (1989). SA: South American Plate; ST: Scotia Plate; AN: Antarctic Plate. The inset shows the location of our study region within South America. b) Map showing our region of interest. The red line represents the MFFS, the white line is the AN-ST subduction trench. Black lines mark the Chile-Argentina border. Red and blue stars (and their corresponding ellipses) show the approximate location of the 1949 Tierra del Fuego events (Castano, 1977; Lomnitz, 1970; Pelayo and Wiens, 1989). Purple dots are seismic events reported by the ISC Catalog. Green and blue dots show the seismsmicity reported by Adaros (2003) and Buffoni et al. (2009), respectively. SP: Southern Patagonia; TdF: Tierra del Fuego. (For interpretation of the references to color in this figure legend, the reader is referred to the Web version of this article.)

approximately constrained to shallow depths, in the western part of the TdF island (Castano, 1977; Lomnitz, 1970; Pelayo and Wiens, 1989) (Fig. 1b).

Paleoseismic observations evidenced a relationship between large magnitude seismic events and the MFFS, during the Quaternary (Costa et al., 2006). Close to the Fagnano lake (western TdF island – Fig. 1b), the displacement associated with the 1949 events was ~4 m. More recent studies show a coseismic displacement of 6.5 m in the eastern part of the TdF island (Roy et al., 2019). Measurements of MFFS coseismic displacement in the Southern Patagonia, to the west, is not obvious especially because of unfavorable topographical and climatic conditions. Nevertheless, structural observations made in the Brunswick Peninsula (Fig. 1) evidence strike slip motion with a NE trend since the Miocene, along the MFFS (Betka et al., 2016).

In this study, we analyze continuous waveforms recorded by broadband seismometers permanently installed in the western Patagonia and TdF island since 2015. We observe P- to S-wave conversions (receiver functions) and the dispersion of earthquake generated surface-waves to constrain the average seismic velocity structure in our study region and use the resulting velocity model to locate the crustal events detected from October 2015 to December 2019. The seismicity is then analyzed in the tectonic framework of the study region as well as previous geological, geodetic and geophysical observations.

2. Geological context

The geology of the study region is rich and quite complex. It shows a remarkable continuity along the MFFS in terms of structure and geological formations (Fig. 2a). In this work, we simplify the configuration by considering 3 main geological units. (1) The Patagonian Batholith (PB), a very important feature characterizing the Southern

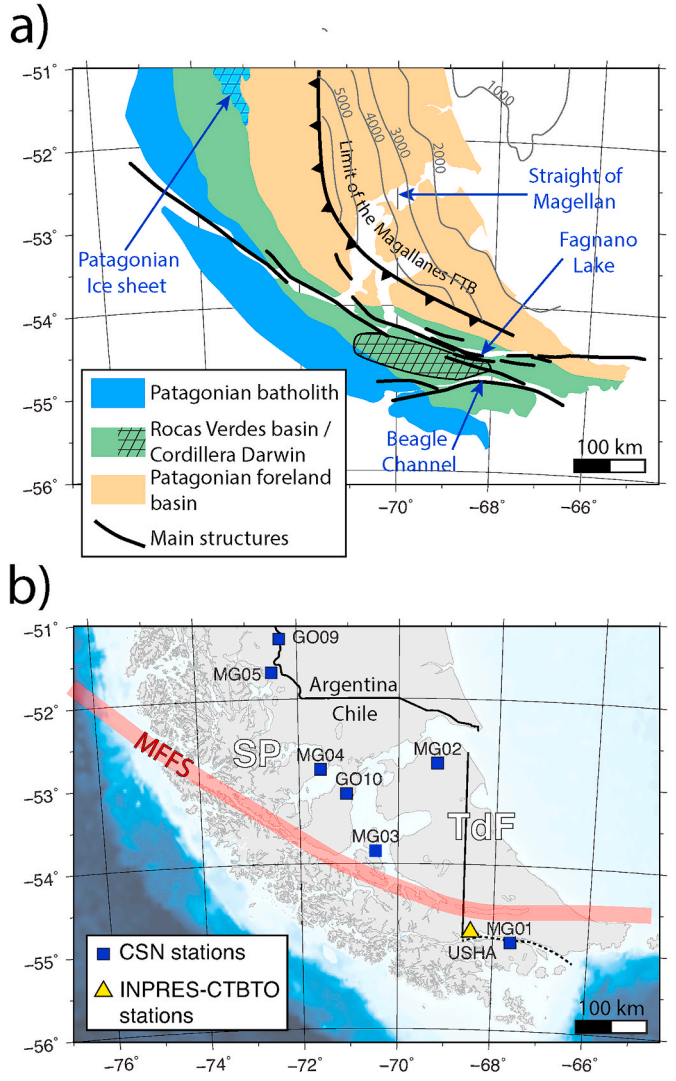

Fig. 2. a) Map showing the principal geomorphological units exposed in the study area (Hervé et al. 2007; Klepeis et al., 2010; Betka et al., 2016). Gray contours show the depth of the Magallanes Foreland basin in meters (Biddle et al., 1986). Black lines show the main structures associated with the MFFS (Betka et al., 2016). b) Map centered on our study area showing the locations of the broadband seismic stations used in this work. Blue squares are permanent stations installed by the Chilean Seismological Center (CSN), Yellow triangle is a permanent station monitored by both the Argentinian Institute for seismic prevention (INPRES) and the Comprehensive Nuclear Test Ban Treaty Organization (CTBTO). The red line represents the MFFS and the black lines correspond to the Chile-Argentina border. (For interpretation of the references to color in this figure legend, the reader is referred to the Web version of this article.)

Andes. It extends from the southernmost tip of South America at 56°S to the north at ~40°S and is related to arc volcanism still active to this day, especially in the northern segment, north of ~46.5°S (GVP, 2020). In the southern segment (our study area), it consists of a series of plutons, mostly granitoids, spanning late Jurassic to Neogene ages (Hervé et al. 2007; Betka et al., 2016). (2) The Rocas Verdes Basin (RVB), exhibits characteristics of an old rift basin with evidence for basaltic magmatism and oceanic crust formation. The rift opened during the Late Jurassic, filling with alteration products coming from the PB and closed prior to ~86 Ma (Klepeis et al., 2010) by underthrusting and obducting the recently formed oceanic floor beneath the South American basement. North of the Beagle Channel, the Cordillera Darwin (CD) is a unique feature in the Southern Andes with a much higher elevation that the rest of the area. It exhibits high grade metamorphic rocks, mostly metasediments interlayered with rocks assemblages in the upper amphibolites facies (Cunningham, 1993; Gombosi et al., 2009), exhumed with the rest of the RVB during the Cretaceous. (3) Finally, the Magallanes Foreland Basin (MFB) covers the northeast part of our study area. Like the rest of the geological features in this area, it shows a NW-SE trend and contains sediment fills with a thickness of more than 6 km (Biddle et al., 1986). Although, filled with detrital material since the Paleozoic, the southern part has been later affected by subsidence and deposition of new sediments from the exhumation of the RVB as well as compressive deformation (Biddle et al., 1986; Klepeis et al., 2010; Fosdick et al., 2011) associated with the late Cretaceous-Neogene Magallanes Fold and Thrust belt (MFTB).

The timing of deformation that affected our study region can be synthetized into 4 major phases: (1) Late Jurassic opening of the RVB. (2) Closure of the RVB during the Mid-Cretaceous followed by the obduction of the RVB oceanic crust over the South American basement and filling of the southern part of the MFB, during the Late Cretaceous. (3) Exhumation of the CD during the Paleogene and NE propagation of the fold and thrust deformation until Eocene-Oligocene. (4) The post Eocene emplacement of the strike-slip deformation related to the MFFS.

3. Previous seismic studies

The first insights about the seismotectonics of the Scotia region were provided by Forsyth (1975) and Pelayo and Wiens (1989). They analyzed the teleseismic waveforms from earthquakes that occurred in this region in order to locate them and estimate their source parameters. These studies helped to constrain the seismicity distribution around the Scotia Plate and contributed to improve the relative plate motion models for this area. In the Southern Patagonia (our study region), their findings were in quite good agreement with previous geological observations and thus confirmed that the MFFS was the western extension of the North Scotia Ridge (Fig. 1). From these 2 studies, it was clear that the seismicity in our study region was far less frequent than observed for the Scotia ridges (both North and South) and especially the South Sandwich trench, much farther to the east (Fig. 1a). Pelayo and Wiens (1989) concluded that the seismicity responsible for the accommodation of the relative plate motions in our study region was “diffuse”, hence not directly associated with any structure.

The seismological instrumentation in our study region began in 1995 with the installation of a permanent seismometer in Ushuaia (Argentina) followed by a small network of five stations that operated in 1997 and 1998 (Robertson et al., 2003). The data from this experiment allowed to constrain a crustal thickness of about 30 km (Lawrence and Wiens, 2004). Using the same data, Adaros (2003) was able to constrain a little less than 150 low magnitude events mainly located in the Southern Patagonia (Fig. 1b). Although the geometrical relationship with the MFFS was not obvious, he concluded that the seismicity was linked to the presence of Riedel faults accommodating crustal deformation, directly related to this structure.

During 2007, five stations operating specifically in Tierra del Fuego (Buffoni et al., 2009) allowed to detect and locate ~180 local seismic events. Buffoni et al. (2009) report that half of this seismicity is characterized by a focal depth comprised between 0 and 10 km (Fig. 1b). However, because this network was only composed of four stations, they also state that the uncertainty increased dramatically for events located far away from the TdF island. Teleseismic receiver function analysis (Buffoni et al., 2019) revealed a crustal thickness for the TdF island ranging from ~25 to ~35 km. The use of short period surface wave dispersion data allowed them to constrain a ~5 km thick sediment layer for the MFB.

The permanent seismological instrumentation of the Southern Patagonia only began after 2011 with the installation of one broadband seismometer in Ushuaia followed by seven broadband seismometers, part of the Chilean Seismic Network (Barrientos et al., 2018).

4. Data and methods

In this work, we analyze seismic data recorded by eight seismometers permanently deployed in the study region (Fig. 2b), between January 2015 and December 2019. Seven of these seismometers were deployed by the Chilean Seismological Center (CSN) in the Southern Patagonia region between 2011 and 2015. Station USHA was deployed in 2011 near Ushuaia, on the south end of the TdF Island. This station is part of the Argentine National Institution for Seismic Prevention (INPRES) network as well as the international monitoring system for the Comprehensive Nuclear-Test-Ban Treaty (CTBTO). These three-components seismometers produce continuous broadband data suitable for both regional and teleseismic observations.

4.1. Regional velocity structure

Waveforms coming from distant earthquakes produce P- to S-wave conversions when crossing seismic velocity discontinuities. When recorded by a multicomponent seismometer, the difference between the direct and converted phase, can be analyzed to investigate the corresponding discontinuity depth as well as the wave propagation speed beneath the seismometer. This operation requires the P-wave signals to be removed from the seismograms producing a receiver function (Langston, 1979), which can be accomplished by deconvolving the vertical component from the radial or tangential components. Because receiver functions (RF) only depend on relative seismic velocity changes, their inversion to solve the velocity structure produces inherent non-unique solutions. To overcome this inconvenience, RF need to be jointly inverted with datasets sensitive to absolute wave velocities such as the dispersion of Rayleigh waves (Julià et al., 2000).

Two hundred twenty-eight teleseismic earthquakes characterized by relatively large magnitude ($M_W > 6$) and epicentral distances between 30° and 90° are cut and band-pass filtered between 0.15 and 5 Hz to remove potential unwanted long-period signals as well as anthropogenic noise (Fig. 3a). Then, the first P-wave arrival is manually picked, which allows us to visually inspect the traces and discard seismograms with low signal-to-noise ratio, recording artifacts, or data gaps. The next step consists in rotating the three-component traces to their respective great circle paths coordinates and compute the RF in the time domain using an iterative method (Ligorria and Ammon, 1999). The deconvolution process is limited to a maximum of 500 iterations or a fit improvement of the RF between two iterations, lower than 0.01%. A Gaussian filter with a width of 2.5 (corresponding to a low pass filter of corner frequency f_c ~ 1.2 Hz) is used to calculate both radial and tangential RF. Once obtained, we perform further quality control of our RF data using the FUNCLAB package (Eagar and Fouch, 2012; Porritt and Miller, 2018). This processing yielded a total of 661 good quality RF (Fig. 3b).

Rayleigh wave dispersion data is estimated following the methodology described in Ammirati et al. (2015). Briefly, a phase match filter (Herrmann, 1973) is applied to a selection of 51 Mw > 6 teleseismic events presenting a high signal to noise ratio (Fig. 3a). This step allows to isolate the fundamental mode from the Rayleigh-wave package within

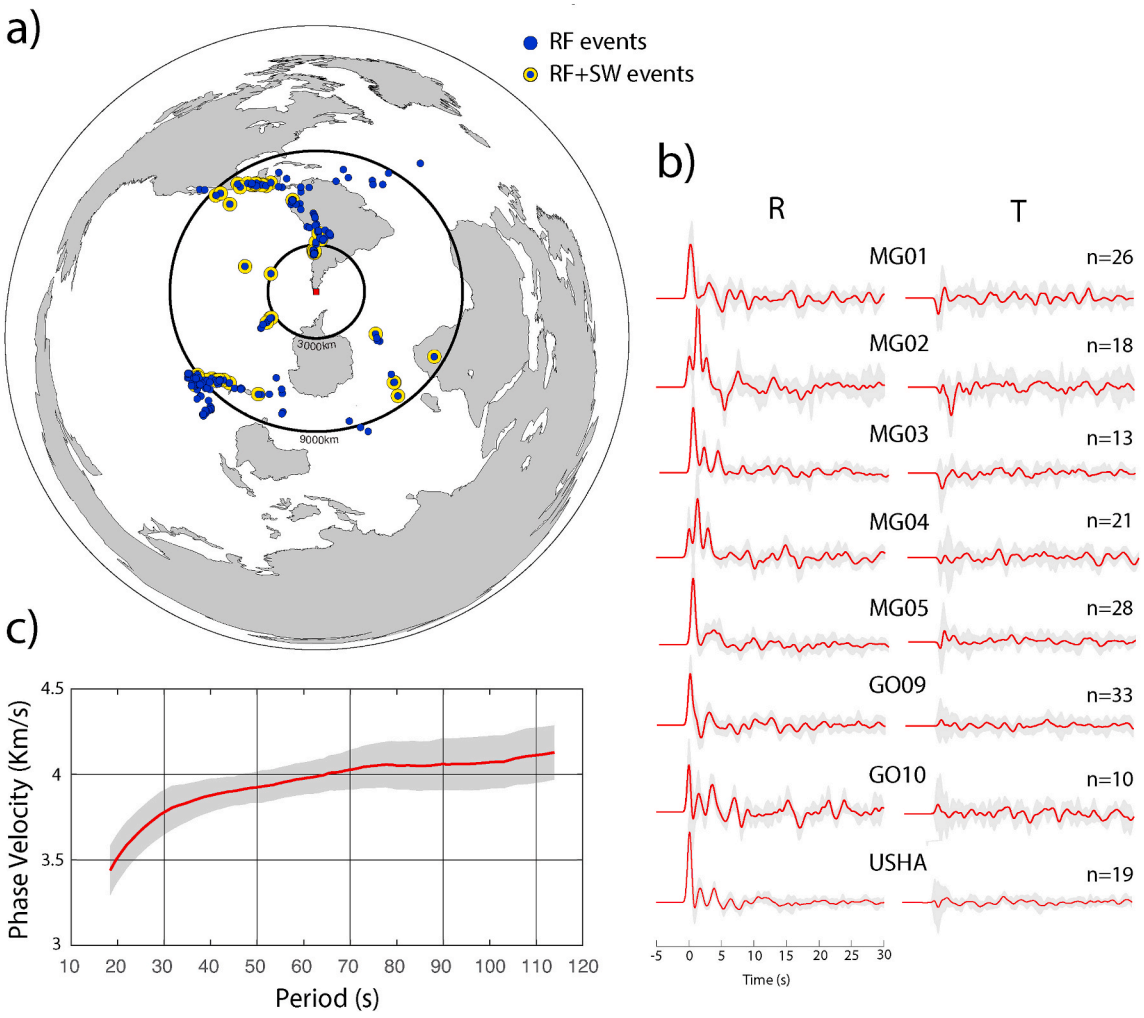

Fig. 3. a) Epicenter location of the teleseismic events used in this work to calculate receiver functions (RF) and Surface wave (SW) dispersion data, blue and yellow circles, respectively. The red square marks the location of our study area. The corresponding waveforms were recorded by the network shown in Fig. 2a b) Radial and tangential RF obtained in this work. Red line is the average RF obtained after moveout correction and stacking. One standard deviation is shown in gray. c) Regional SW phase velocity dispersion obtained in this work (red line) with 1 standard deviation confidence interval (gray envelope). (For interpretation of the references to color in this figure legend, the reader is referred to the Web version of this article.)

the 15–120 s period, thus discarding any interference caused by the body waves. Then we apply a frequency domain wavefield transformation method (McMechan and Yeldin, 1981) to calculate an average dispersion curve for the entire network. Using this methodology, we obtain 51 dispersion curves (one for each event). The final regional dispersion curve is obtained by stacking those curves (Fig. 3c).

Both RF and Rayleigh wave dispersion datasets are then jointly inverted using the joint96 code (Julià et al., 2000; Herrmann and Ammon, 2002) for which a multilayer initial velocity model is iteratively altered in order to fit both datasets. Our initial velocity model consisted in 45 layers that resemble the AK135 Earth model (Kennett et al., 1995) wave velocities, down to 225 km depth. Each dataset accounts for 50% in the joint inversion. In practice, giving more weight to the RF dataset can result in more detailed velocity structures whereas more weight given to the surface wave dataset will result in smoother velocity variations. Considering the size of our study region and the consequent spacing between our stations, as well as possible lateral heterogeneities between the stations, we are not in the position to obtain detailed velocity variations. This would require a greater number of stations and a much denser distribution. In this work, we constrain regional crustal and upper mantle velocities as well as the regional crustal thickness. For a given station, the corresponding RF are jointly inverted with the regional surface wave data producing a 1D velocity model for that station. Thus, eight velocity models are obtained (one for each station) and the final regional velocity model corresponds to the average of these models (Fig. 4 & Table S1).

4.2. Earthquake detection and source characterization

For event detection, we analyze daily continuous records previously high-pass filtered with a corner frequency $f_c = 4$ Hz, discarding events coming from teleseismic distances and apply a short-term averaging/long-term averaging (STA/LTA) coincidence trigger (Fig. S1). Because of the limited number of stations and their scarce spacing, we increase the trigger sensitivity and set a minimum number of stations to three. This criterion resulted in the detection of 403 local earthquakes, occurred between October 2013 and December 2019.

These events are then visually inspected to discard eventual false positives and manually pick P- and S-waves phases. Earthquakes recorded by less than four stations are systematically discarded. Events with a minimum of four picks (including at least one S phase) are located using the NonLinLoc code (Lomax et al., 2000). This non-linear, grid--search method is based on the probabilistic formulation of inverse problems described in Tarantola and Valette (1982) where error of observations (phases picks) and travel time calculations, are assumed to be Gaussian. This allows the analytic calculation of a maximum likelihood

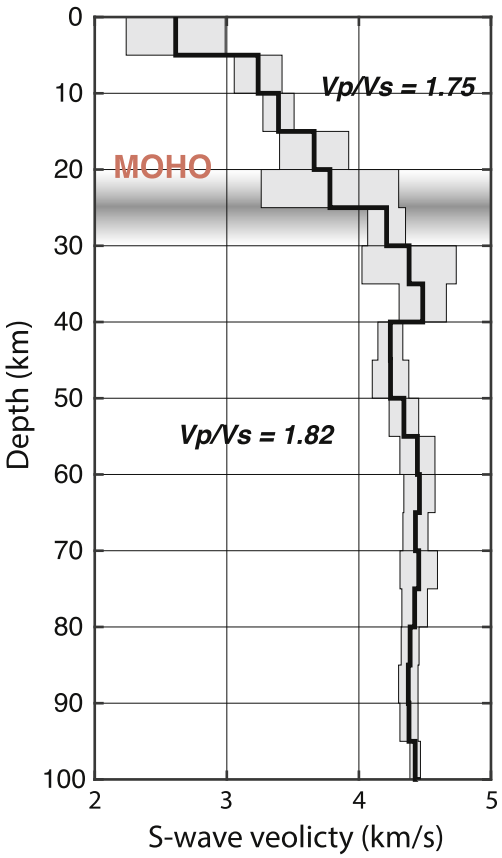

Fig. 4. regional velocity model obtained from the joint inversion of RF and SW phase velocity dispersion. Black line is the average shear wave velocity and the gray envelope shows its variations for each layer, within 1 standard deviation. The regional Moho is interpreted between 25 and 30 km (see main text).

origin time from the observed arrival times and the calculated travel times between the receivers and a specific point in space. The resulting hypocenters are represented by a probability density function allowing more comprehensive uncertainty estimations. P- and S-wave travel times are calculated for the velocity model obtained from our RF and surface wave joint inversion (Fig. 4). Once located, the local magnitude (M_L) for each event is estimated based on waveform maximum amplitudes.

5. Results and interpretations

Although our network does not allow to make detailed interpretations about the wave velocity variations and their lateral extents, the RF-Rayleigh wave dispersion joint inversion gives some insights about the average velocity variations with depth for our study region. The uncertainties on the velocity model cause differences in time up to 0.13 s when migrating from time to depth (Gurrola et al., 1994). Considering an average crustal shear wave velocity of 3.33 km/s and an average mantle shear wave velocity of 4.1 km/s leads to uncertainty on depth estimations of about 4 km at 25 km depth and 10 km at 100 km depth. For this reason, the 5-km depth increment in our velocity model is adequate for the purposes of this study.

The first layer corresponding to depths ranging from 0 to 5 km is characterized by a shear wave velocity of 2.6 km/s. Such low velocities are common at thiese depths and usually correspond to altered minerals and/or sedimentary fills with high water content. In our case, they would characterize the MFB and the deformed Jurassic-Cretaceous sequences of the MFTB (Fig. 2). From 5 to 20 km, the velocity gradually increases from 3.2 km/s to 3.8 km/s. This velocity range can be associated with a broad range of felsic metamorphic and/or non-metamorphic rocks that could characterize the Magallanes foreland and Rocas Verdes pre-Jurassic basements. (Christensen and Mooney, 1995, Fig. 2).

A typical Quartz-enriched continental crust is composed of ~60% of SiO_2 (Christensen and Mooney, 1995). In this case, the transition from brittle to plastic deformation is expected to occur between 10 and 20 km, depending on P-T conditions. Our regional velocity model seems to exhibit a small crustal discontinuity at 15 km depth where the velocity jumps from 3.4 to 3.7 km/s, which could correspond to the brittle-ductile transition. Finally, we observe a clear increase in seismic velocities at 25 km with a jump from 3.8 to 4.2 km/s likely associated with the transition from lower crust rocks (granulite facies) and the upper mantle characterized by ultramafic compositions. These observations thus suggest that the crustal thickness in our study region is 25–30 km. These values are consistent with previous crustal thickness estimations from Adaros (2003) and Buffoni et al. (2019). Interestingly, the crustal thickness in our study area represents a much lower value than the world average of 40 km (Christensen and Mooney, 1995).

In this study, we obtained a total of 163 hypocenters corresponding to events occurred between October 2015 and December 2019 (Fig. 5 & Table S2). Location errors are estimated from the 68% confidence ellipsoid calculated from the samples of the location probability density function. As mentioned before, due to the limited number of stations available as well as their scarce spacing, the volume of the ellipsoids can be considerable and thus results in quite high uncertainties. The average horizontal error is $h_{err} = 27$ km with a standard deviation of $\sigma = 19$ km and the vertical error is $z_{err} = 25$ km ($\sigma = 13$ km). The average root mean square (RMS) is 0.4 s ($\sigma = 0.2$ s), an acceptable value considering the configuration of the network (Figs. 2b and 5b).

As previously mentioned, the average crustal thickness estimated for the study region is about 25–30 km. The standard deviation associated with our hypocenters is about the same order. This is because some events are very badly constrained, with large uncertainties. Discarding all events with hypocenters deeper than 30 km and vertical uncertainty greater than 30 km, results in 82 events with an average focal depth of 8 km ($\sigma = 7.6$ km). The depth uncertainty decreases considerably, down to 15 km ($\sigma = 9$ km). Thus, we are confident that these hypocenters correspond to crustal events.

In general, we observe a fair number of hypocenters distributed along the MFFS. In the northern section (Fig. 5), we note the presence of many events with a more diffuse distribution within the crust, bounded to the east by the front of the MFTB. Local magnitudes associated with the events characterized in this work, range from $1.9 < M_L < 5.3$. Interestingly, we note that higher magnitude events are located closer to the fault whereas small magnitude events are rather associated with hypocenters located in the northern part of the MFTB (Fig. 5). This observation indicates that more seismic moment is released by the MFFS than the MFTB. However, it is important to point out that our stations are mainly located on the MFTB (Fig. 2), thus they are more likely to detect smaller magnitude events occurring in this sector. On the other hand, there is no doubt that more stations located closer to the MFFS would yield a greater number of events.

6. Discussion

The seismicity characterized in this work reveals two separates mechanisms of crustal deformation in our study area. On one side, we observed events aligned along the MFFS that correlate quite well with GNSS measurements and global plate motion models (Fig. 6a) as well as the markers of deformation indicating seismic activity during the Quaternary. This leaves little doubt that the transcurrent deformation that accommodates the relative movement between the Scotia Plate and the South American Plate is an ongoing process. Fault slip data collected in the MFTB, in the Brunswick Penisula area shows a series of NW trending strike slip faults sometimes associated with E-NE normal faults parallel

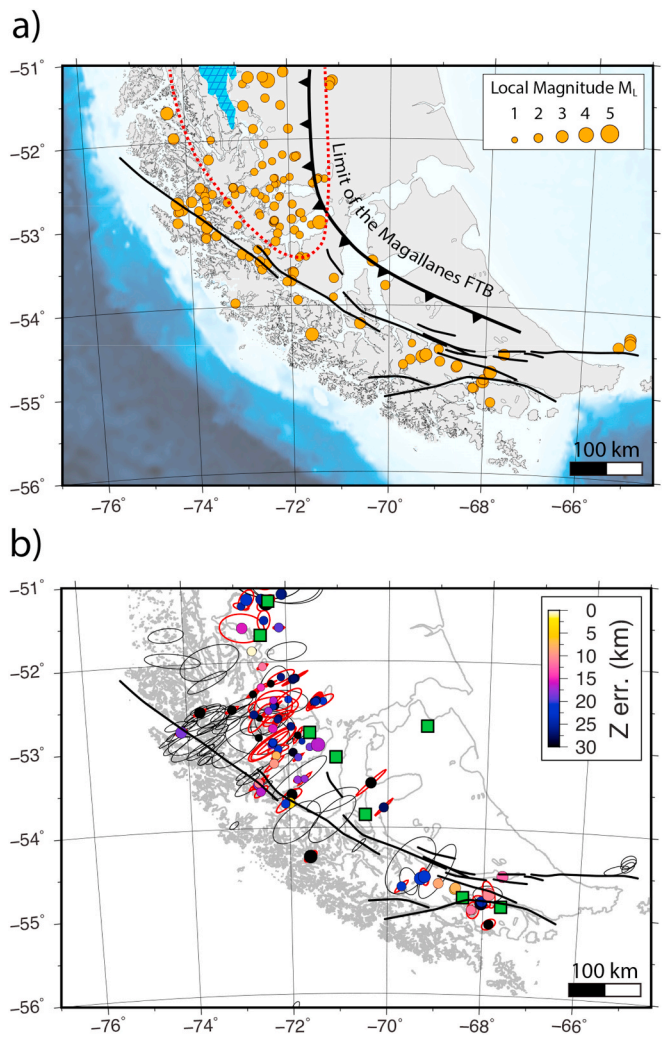

Fig. 5. a) Epicentral distribution of the seismicity characterized in this work. The circle sizes are proportional to the local magnitude (M_L). Main structures associated with the MFFS (Betka et al., 2016) are represented by the black lines. The thick black line with arrows shows the limit of the Magallanes fold and thrust belt (Fosdick et al., 2011). Note how the seismicity is broadly aligned with the MFFS. North of 53.5°S, the seismicity seems more diffuse within the crust (red dashed line). The Patagonian ice sheet appears north of 52°S (blue hatched polygon). b) Uncertainties associated with the events showed in a). red ellipses correspond to the horizontal uncertainties for a selection of events with focal depths lower than z = 30 km and a depth uncertainty lower than $z_{err} < 30$ km (see main text and Table S2). The dots show the best location associated with this selection of events for which the color is proportional to the vertical error (z_{err}). Black ellipses show the horizontal uncertainties associated with the rest of the events characterized in this work (Table S2). Green squares refer to seismic station locations (Fig. 2b). (For interpretation of the references to color in this figure legend, the reader is referred to the Web version of this article.)

with older structures (reverse faults and compressional folds) related to the MFTB, compatible with regional bulk transtension. This set of structures is kinematically compatible with the sinistral character of the MFFS. Interestingly, they crosscut or reactivate reverse faults and folds of the MFTB, confirming that the strike-slip deformation, postdates the Late-Cretaceous-Eocene folding and thrusting (Betka et al., 2016). This information thus suggests that the displacement along the MFFS began in response to the opening of the west Scotia sea and the Drake passage during the early Miocene. It is also a perfect example of how strike-slip motion at crustal scale can reactivate a preexisting fault and thrust belt. Since there are no markers of NE crustal shortening after the Eocene, we can reasonably believe that the strike slip accommodation between the Scotia and the South American plates became the dominant motor of deformation since ~20 Ma. The seismic activity along the MFFS found in this work demonstrates that this is still the case in the present days (Fig. 6).

In the South TdF region, the MFFS strikes almost 90° and exhibits the same parallelism with the Late-Cretaceous-Eocene fold and thrust belt structure (Ghiglione and Ramos, 2005; Klepeis and Austin, 1997). Besides the evidence for coseismic displacements during the Pleistocene, Roy et al. (2019) found the presence of Riedel faults characterized with an uplifted southern block, on most of the MFFS segments in the area. This is interesting because this observation can be combined with an increase of crustal seismic activity observed beneath the Darwin Cordillera in this work and also in previous seismic studies such as Buffoni et al. (2009) that specifically analyzed seismic data recorded by stations installed in the TdF island (Figs. 1 and 5). We do not discard that the Fuegino volcano could also generate some seismic activity in this area (Fig. 6a). Mendoza et al. (2011) observed an uplift of 3 mm/yr west of 67.5°W in an area comprised between the Fagnano lake and the Beagle channel, where the Cordillera Darwin lies. There is a possibility that isostatic rebound due to the retreat of the Patagonian Ice sheet for the last ~16 ky contributes to the crustal deformation in the CD area, in addition to the strike-slip deformation induced by the MFFS (Fig. 6b). The fact that the Beagle channel is a former glacial valley indicates that the area was completely covered in ice during the last glacial maximum, ~20–22 ka with an ice retreat starting ~14–16 ka (Rabassa et al., 1990; 2006).

The crustal seismicity located north of our study region (between 51°-53°S and 71°-73°W), within the Magallanes FTB (Fig. 5) seems disconnected from the MFFS. In this sector, the MFTB structures display an almost N–S orientation, sub-parallel to the subduction trench (Fig. 6a). The presence of an active volcanic arc and a trench-parallel FTB indicates an increasing influence of the subduction in the crustal deformation process in this area (51-53°S). Possibly the seismic activity observed between 51 and 53°S is related to this deformation although stratigraphic/structural analysis and U/Pb ages (Fosdick et al., 2011) demonstrated that the MFTB accommodated most of its shortening from 80 to 20 Ma. Another possible explanation for the increased seismicity north of 51°S could be the isostatic rebound from the retreat of the Patagonian ice sheet as also suggested for the Cordillera Darwin, to the south. We note that the Southern Andes between 49 and 52°S are still covered with what remains of the Patagonian ice sheet (Fig. 2a). Over the years, it became clear that the ice mass significantly decreased due to a global temperature rise during the Holocene, since the end of the last glacial period. In the Southern Patagonia, an ice loss rate of ~17 km^3/yr has been estimated from satellite observations of glacier topography, for the 1960–2000 period (Rignot et al., 2003). Crustal uplift due to changes in ice mass has been observed all over the world but in particular in mountain ranges of Northern Europe and North America (Fennoscandia and Laurentia, respectively) where present day vertical motion can reach 16 mm/yr (Lidberg et al., 2007; Sella et al., 2007). Geodetic observations in Southern Patagonia between 2003 and 2006 evidenced an uplift velocity rate ranging from 23 to 39 mm/yr, with higher rates above the remaining ice sheet (Dietrich et al., 2010). These values are significantly higher than the one observed in for the CD, south of the TdF Island (Mendoza et al., 2011) and there is a possibility that most of the crustal seismicity observed north of 53°S, is mainly related to this mechanism of crustal deformation (Fig. 6c).

7. Concluding remarks

In this work, we processed continuous waveforms recorded by eight permanent broadband stations installed in the Southern Patagonia and Tierra del Fuego areas. The joint inversion of teleseismic receiver functions and Rayleigh wave dispersion from distant earthquake estimations allowed us to estimate the regional seismic wave velocity structure and a crustal thickness of 25–30 km. Using the obtained

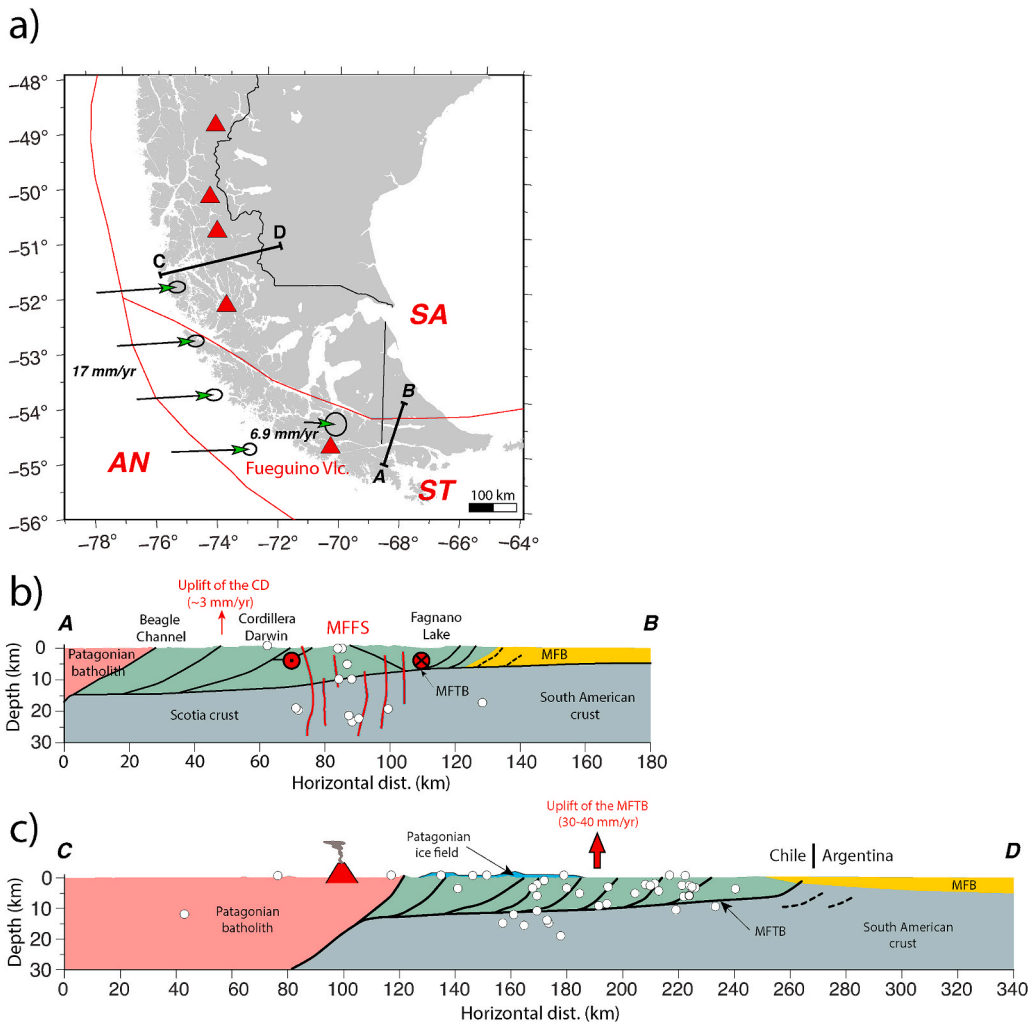

Fig. 6. a) Map showing tectonic boundaries characterizing our study area (red lines). The vectors show the displacement direction and velocity rates for the Antarctic Plate (AN) and the Scotia Plate (ST) relative to the South American Plate (SA). These vectors were calculated by averaging various plate motion models (Unavco, 2020). Straight black lines show the location of cross sections AB and CD. Red triangle marks the location of the subduction related active volcanoes (GVP, 2020). b) Cross section AB. The white dots represent the hypocenters with a vertical error lower than $z_{err} <$ 30 km (Fig. 5 and Table S2). Note that in this sector, the crustal seismicity associated with the Magallanes-Fagnano fault system (MFFS). The structures (black lines) has been schematized from Klepeis et al. (2010). c) Cross section CD. Same as b) expect in this case, the seismicity is rather associated with the reactivation of the Magallanes fold and thrust belt (MFTB) possibly due to the retreat of the Patagonian Ice sheet. The structures (clack lines) has been schematized from Fosdick et al. (2011). (For interpretation of the references to color in this figure legend, the reader is referred to the Web version of this article.)

velocity structure, we localized 163 crustal earthquakes. The seismicity characterized in our study region shows a good correlation with the presence of the Magallanes fault system and suggests that this structure is the principal mechanism of crustal deformation, especially in the south Tierra del Fuego region. More to the north, along the Patagonian Andes and the Magallanes fold and thrust belt, we observed the presence of more diffuse seismicity at crustal level. This observation combined with evidence of rapid crustal uplift from other studies, drives to the hypothesis of isostatic rebound due to the retreat of the Patagonian ice sheet as a major crustal deformation mechanism for the past ~16 ky.

We acknowledge that our network configuration is far from ideal for getting fine details about crustal velocity structure variations as well as their lateral extents. Moreover, the station spacing is quite important and does not allow optimal hypocenter determination. However, for the first time, we are able to obtain interesting insights about the regional seismicity characterizing Magallanes Fagnano Fault area. In the future, more seismic stations, with a denser distribution around the MFFS, as well as new GNSS measurements will allow to considerably refine the results presented in this manuscript.

CRediT authorship contribution statement

Jean-Baptiste Ammirati: Conceptualization, Methodology, Formal analysis, Writing - original draft. **M. Constanza Flores:** Methodology, Resources, Writing - review & editing. **Sergio Ruiz:** Conceptualization, Writing - review & editing.

Declaration of competing interest

The authors declare that they have no known competing financial interests or personal relationships that could have appeared to influence the work reported in this paper.

Acknowledgements

The authors thank the CSN team as well as the IRIS-DMC for facilitating the access to the seismic waveforms used in this work. This research was supported by the Universidad de Chile through the Programa Riesgo Sísmico - Actividades de Interés Nacional (AIN). J.-B.A. is funded by the Agencia Nacional de Investigación y Desarollo of Chile (ANID) through the Fondo de desarollo Científico y técnico program (FONDECYT N°3200633). Seismic data were prepared using SAC and processed using the Computer Programs in Seismology (CPS version 3.30). Most of the figures present in this paper were made with GMT (version 6.0). We would like to thank the editor, Andrés Folguera as well as the two anonymous reviewers for their very helpful comments on the original article.

Appendix A. Supplementary data

Supplementary data to this article can be found online at https://doi.org/10.1016/j.jsames.2020.102799.

References

Adaros, R.E., 2003. Sismicidad y tectónica del extremo sur de Chile. Dissertation of the Universidad de Chile. Facultad de ciencias físicas y matemáticas, Departamento de Geofísica, Santiago, Chile.

Ammirati, J.-B., Alvarado, P., Beck, S., 2015. A lithospheric velocity model for the flat slab region of Argentina from joint inversion of Rayleigh wave phase velocity dispersion and teleseismic receiver functions,. Geophys. J. Int. 202, 224–241. https://doi.org/10.1093/gji/ggv140.

Barrientos, S., 2018. The seismic network of Chile. Seismol Res. Lett. 89 (2A), 467–474. https://doi.org/10.1785/0220160195. National Seismological Center (CSN) Team.

Betka, P., Klepeis, K., Mosher, S., 2016. Fault kinematics of the Magallanes-Fagnano fault system, southern Chile: an example of diffuse strain and sinistral transtension along a continental transform margin. J. Struct. Geol. 85, 130–153. https://doi.org/10.1016/j.jsg.2016.02.001.

Biddle, K.T., Uliana, M.A., Mitchum Jr., R.M., Fitzgerald, M.G., Wright, R.C., 1986. The stratigraphic and structural evolution of the central and eastern Magallanes Basin, southern South America, Spec. Publsint. Ass. Sediment 8, 41–61.

Buffoni, C., Sabbione, N.C., Connon, G., Ormaechea, J.L., 2009. Localización de hipocentros Y Determinación de su magnitud en Tierra del Fuego Y zonas Aledañas. Geoacta 34, 75–86.

Buffoni, C., Schimmel, M., Sabbione, N.C., Rosa, M.L., Connon, G., 2019. Crustal structure beneath Tierra del Fuego, Argentina, inferred from seismic P-wave receiver functions and ambient noise autocorrelations. Tectonophysics 751, 41–53. https://doi.org/10.1016/j.tecto.2018.12.013.

Caminos, R., Haller, M., Lapido, O., Lizuain, A., Page, R., Ramos, V., 1981. Reconocimiento geológico de los Andes Fueguinos, Territorio Nacional de Tierra del Fuego. 8° Congreso Geológico Argentino. Acta 3, 759–786.

Castano, J.C., 1977. Zonificación sísmica de la República Argentina. Publicación Técnica 5, 40.

Christensen, N.I., Mooney, W.D., 1995. Seismic velocity structure and composition of the continental crust: a global view. J. Geophys. Res. 100, 9761–9788. https://doi.org/10.1029/95JB00259.

Cisternas, A., Vera, E., 2008. Sismos históricos y recientes en Magallanes. Magallania 36, 43–51. https://doi.org/10.4067/S0718-22442008000100004.

Costa, C.H., Smalley, R., Schwartz, D.P., Stenner, H.D., Ellis, M., Ahumada, E.A., Velasco, M.S., 2006. Paleoseismic observations of onshore transform boundaries: the Magallanes-Fagnano fault, Tierra del Fuego, Argentina,. Rev. Asoc. Geol. Argent. 61 (4), 647–657.

Cunningham, W.D., 1993. Strike-slip faults in the southernmost Andes and the development of the patagonian orocline. Tectonics 12 (1), 169–186. https://doi.org/10.1029/92TC01790.

Dietrich, R., Ivins, E.R., Casassa, G., Lange, H., Wendt, J., Fritsche, M., 2010. Rapid crustal uplift in Patagonia due to enhanced ice loss., Earth Planet. Sc. Lett.289 22–29. https://doi.org/10.1016/j.epsl.2009.10.021.

Eagar, K.C., Fouch, M.J., 2012. FuncLab: a MATLAB interactive toolbox for handling receiver function datasets. Seismol Res. Lett. 83 (3), 596–603. https://doi.org/10.1785/gssrl.83.3.596.

Forsyth, D.W., 1975. Fault plane solutions and tectonics of the south atlantic and Scotia sea, J. Geophys. Res. 80 (11), 1429–1443. https://doi.org/10.1029/JB080i011p01429.

Fosdick, J.C., Romans, B.W., Fildani, A., Bernhardt, A., Calderón, M., Graham, S.A., 2011. Kinematic evolution of the Patagonian retroarc fold-and-thrust belt and Magallanes foreland basin, Chile and Argentina, 51°30′S. Geol. Soc. Am. Bull. 123 (9–10), 1679–1698. https://doi.org/10.1130/B30242.1.

Fuenzalida, R.H., 1976. The magellan fault zone, symposium on andean and antarctic volcanology problems. In: Int. Assoc.. Of Volcanol. and Chem.. of the Earth's Inter., Naples, Italy.

Geller, R.J., Kanamori, H., 1977. Magnitude of great shallow earthquakes from 1904 to 1952. Bull. Seismol. Soc. Am. 67 (3), 587–598.

Ghiglione, M.C., Ramos, V.A., 2005. Progression of deformation and sedimentation in the southernmost Andes. Tectonophysics 405, 25–46. https://doi.org/10.1016/j.tecto.2005.05.004.

GVP (Global Volcanism Program), 2020. Smithsonian Institution, National Museum of Natural History – List of Holocene volcanoes. https://volcano.si.edu/list_volcano_holocene.cfm.

Gombosi, D.J., Barbeau Jr., D.L., Garver, J.I., 2009. New thermochronometric constraints on the rapid Palaeogene exhumation of the Cordillera Darwin complex and related thrust sheets in the Fuegian Andes. Terra. Nova 21, 507–515. https://doi.org/10.1111/j.1365-3121.2009.00908.x.

Gurrola, H., Minster, J.B., Owens, T., 1994. The use of velocity spectrum for stacking receiver functions and imaging upper mantle discontinuities. Geophys. J. Int. 117, 427–440. https://doi.org/10.1111/j.1365-246X.1994.tb03942.x.

Herrmann, R.B., 1973. Some aspects of band-pass filtering of surface waves, Bull.. seism. Soccer Am. 63, 703–711.

Herrmann, R.B., Ammon, C.J., 2002. Computer programs in seismology— 3.30: surface waves, receiver functions and crustal structure. Available at: http://www.eas.slu.edu/eqc/eqccps.html.

Hervé, F., Pankhurst, R.J., Fanning, C.M., Calderón, M., Yaxley, G.M., 2007. The South Patagonian Batholith: 150 My of granite magmatism on a plate margin. Lithos 97, 373–394. https://doi.org/10.1016/j.lithos.2007.01.007.

ISC, 2020. International seismological centre – search the ISC bulletin. https://doi.org/10.31905/D808B830.

Julià, J., Ammon, C.J., Herrmann, R.B., Correig, A.M., 2000. Joint inversion of receiver function and surface wave dispersion observations. Geophys. J. Int. 143, 99–112. https://doi.org/10.1046/j.1365-246x.2000.00217.x.

Kennett, B.L.N., Engdahl, E.R., Buland, R., 1995. Constraints on seismic velocities in the Earth from traveltimes. Geophys. J. Int. 122, 108–124. https://doi.org/10.1111/j.1365-246X.1995.tb03540.x.

Klepeis, K.A., Austin, J.A., 1997. Contrasting styles of superposed deformation in the southernmost Andes. Tectonics 16 (5), 755–776. https://doi.org/10.1029/97TC01611.

Klepeis, K., Betka, P., Clarke, G., Fanning, M., Hervé, F., Rojas, L., Mpodozis, C., Thomson, S., 2010. Continental underthrusting and obduction during the cretaceous closure of the Rocas Verdes rift basin, Cordillera Darwin, patagonian Andes. Tectonics 29, TC3014. https://doi.org/10.1029/2009TC002610.

Langston, C.A., 1979. Structure under Mount Rainier, Washington, inferred from teleseismic body waves. J. Geophys. Res. 84, 4749–4762. https://doi.org/10.1029/JB084iB09p04749.

Lawrence, J.F., Wiens, D.A., 2004. Combined receiver-function and surface wave phase-velocity inversion using a niching genetic algorithm: application to Patagonia. Bull. Seismol. Soc. Am. 94 (3), 977–987. https://doi.org/10.1785/0120030172.

Lidberg, M., Johansson, J., Scherneck, H.-G., Davis, J., 2007. An improved and extended GPS-derived 3D velocity field of the glacial isostatic adjustment (GIA) in Fennoscandia. J. Geodyn. 81 (3), 213–230. https://doi.org/10.1007/s00190-006-0102-4.

Ligorría, J., Ammon, C.J., 1999. Iterative deconvolution and receiver function estimation. Bull. Seismol. Soc. Am. 89, 1395–1400.

Lodolo, E., Menichetti, M., Bartole, R., Ben- Avraham, Z., Tassone, A., Lippai, H., 2003. Magallanes-Fagnano continental transform fault (Tierra del Fuego, southernmost South America). Tectonics 22 (6). https://doi.org/10.1029/2003TC001500.

Lomax, A., Virieux, J., Volant, P., Berge, C., 2000. Probabilistic earth- quake location in 3D and layered models: introduction of a Metropolis- Gibbs method and comparison with linear locations. In: Thurber, C.H., Rabinowitz, N. (Eds.), Advances in Seismic Event Location. Kluwer, Amsterdam, The Netherlands, pp. 101–134.

Lomnitz, C., 1970. Major earthquakes and tsunamis in Chile during the period 1535 to 1955. Geol. Rundsch. 59, 938–960. https://doi.org/10.1007/BF02042278.

McMechan, G.A., Yeldin, J., 1981. Analysis of dispersive waves by wave field transformation. Geophysics 46, 869–874. https://doi.org/10.1190/1.1441225.

Mendoza, L., Perdomo, R., Hormaechea, J.L., Cogliano, D.D., Fritsche, M., Richter, A., Dietrich, R., 2011. Present-day crustal deformation along the Magallanes-Fagnano Fault System in Tierra del Fuego from repeated GPS observations. Geophys. J. Int. 184, 1009–1022. https://doi.org/10.1111/j.1365-246X.2010.04912.x.

Mendoza, L., Richter, A., Fritsche, M., Hormaechea, J.L., Perdomo, R., Dietrich, R., 2015. Block modeling of crustal deformation in Tierra del Fuego from GNSS velocities. Tectonophysics 651–652, 58–65. https://doi.org/10.1016/j.tecto.2015.03.013.

Pelayo, A.M., Wiens, D.A., 1989. Seismotectonics and relative plate motions in the Scotia Arc region. J. Geophys. Res. 94, 7293–7320. https://doi.org/10.1029/JB094iB06p07293.

Porritt, R.W., Miller, M.S., 2018. Updates to FuncLab, a Matlab based GUI for handling receiver functions. Comput. Geosci. 111, 260–271. https://doi.org/10.1016/j.cageo.2017.11.022.

Rabassa, J., Serrat, D., Marti, C., Coronato, A., 1990. El Tardiglacial en el Canal Beagle, Tierra del Fuego, Argentina.XI Congreso Geológico Argentino. Acta 1, 290–293 (SanJuan).

Rabassa, J., Coronato, A., Heusser, C., RoigJuñet, F., Borromei, A., Roig, C., Quattrocchio, M., 2006. The peatlands of Argentine Tierradel Fuego as a source for paleoclimatic and paleo environmental information. In: Martini, I., Martínez Cortizas, A., Chesworth, W. (Eds.), Peatlands: Evolution and Records of Environmental and Climate Changes. Elsevier, pp. 129–144.

Rignot, E., Rivera, A., Casassa, G., 2003. Contribution of the Patagonia icefields of South America to global sea level rise. Science 302, 434–437. https://doi.org/10.1126/science.1087393.

Robertson, M.S., Wiens, D.A., Koper, K.D., Vera, E., 2003. Crustal and upper mantle structure of southernmost South America inferred from regional waveform inversion. J. Geophys. Res. 108 (B1), 2038. https://doi.org/10.1029/2002JB001828.

Roy, S., Vassallo, R., Martinod, J., Ghiglione, M.C., Sue, C., Allemand, P., 2019. Co-seismic Deformation and Post-glacial Slip along the Magallanes-Fagnano Fault, vol. 32. Tierra Del Fuego, Argentina, Terra Nova, pp. 1–10. https://doi.org/10.1111/ter.12430, 1.

Sandoval, F.B., De Pascale, G.P., 2020. Slip rates along the narrow Magallanes fault system, Tierra del Fuego region, vol. 10. Sci. Rep, Patagonia. https://doi.org/10.1038/s41598-020-64750-6, 8180.

Sella, G., Stein, S., Dixon, T., Craymer, M., James, T., Mazzotti, S., Dokka, R., 2007. Observation of glacial isostatic adjustment in "stable" North America with GPS. Geophys. Res. Lett. 34, L02306. https://doi.org/10.1029/2006GL027081.

Smalley Jr., R., Kendrick, E., Bevis, M., Dalziel, I., Taylor, F., Lauría, E., Barriga, R., Casassa, G., Olivero, E., Piana, E., 2003. Geodetic determination of relative plate motion and crustal deformation across the Scotia-South America plate boundary in eastern Tierra del Fuego. G-cubed 4 (9). https://doi.org/10.1029/2002GC000446.

Tarantola, A., Valette, B., 1982. Generalized nonlinear inverse problems solved using the least squares criterion. Rev. Geophys. 20 (2), 219–232. https://doi.org/10.1029/RG020i002p00219.

Unavco, 2020. Plate motion calculator. https://www.unavco.org/software/geodetic-utilities/plate-motion-calculator/plate-motion-calculator.html.

Winslow, M., 1982. The structural evolution of the Magallanes basin and neotectonics of the southernmost Andes. In: Craddock, C. (Ed.), Antarctic Geoscience. University of Wisconsin, pp. 143–154.